Electrode work function engineering with phosphonic acid monolayers and molecular acceptors: Charge redistribution mechanisms

Melanie Timpel,[†§Δ] Hong Li,[~Δ*] Marco V. Nardi,[†§] Berthold Wegner,[†‡] Johannes Frisch,[†‡] Stephen Barlow,[~] Jean-Luc Brédas,[~] and Norbert Koch[†‡⊥]*

[†]Institut für Physik, Humboldt-Universität zu Berlin, Newtonstr. 15, 12489 Berlin (Germany)

[§]IMEM-CNR Institute, Via alla Cascata 56/C, Povo – 38123 Trento (Italy)

[~]Center for Organic Photonics and Electronics (School of Chemistry and Biochemistry, Georgia Institute of Technology, Atlanta (USA)

[‡]Helmholtz-Zentrum Berlin für Materialien und Energie GmbH, Albert-Einstein-Str. 16, 12489 Berlin (Germany)

[⊥]Jiangsu Key Laboratory for Carbon Based Functional Materials and Devices and Institute of Functional Nano and Soft Materials (FUNSOM), Soochow University, 199 Ren-Ai Road, Suzhou 215123 (China)

KEYWORDS: self-assembled monolayer; phosphonic acid; ITO; photoelectron spectroscopy; density-functional theory

ABSTRACT

Employing self-assembled monolayers (SAMs) of dipolar molecules or adsorbed molecular acceptors on electrode materials are common strategies to increase the work function, thereby facilitating good hole injection into an organic semiconductor. Here we show that a combination of both approaches can possibly surpass the performance of the individual ones. By combined experimental and theoretical methods we reveal that in a three-component system, consisting of an indium-tin-oxide (ITO) electrode, a carbazole-based phosphonic acid SAM, and a molecular acceptor layer atop, charge transfer occurs from the ITO to the acceptor layer associated with an electrostatic field drop over the charge-neutral SAM. This result is in contrast to common expectations of p-doping of the SAM by the acceptor molecules. High work function values of 5.7 eV were achieved with this system, which may be increased by exploiting the identified fundamental charge redistribution mechanisms with other material combinations.

INTRODUCTION

The strong molecular electron acceptor tetrafluoro-tetracyanoquinodimethane (F_4TCNQ, molecular structure given in Figure 1a) has been shown to modify the energy level distribution when it forms interfaces with metal,[1–3] graphene,[4,5] and metal oxide[6–8] electrodes, where it also increases the work function (Φ). Because of its strong electron accepting nature, F_4TCNQ likewise acts as a p-type dopant for many organic semiconductors.[6,9–11] Although the p-doping of bulk

organic semiconductors has been intensively studied over the past few years, mainly in the context of organic opto-electronic applications,[12] the impact of a strong electron acceptor on a self-assembled monolayer (SAM) exhibiting a π-conjugated organic moiety as used in advanced surface modification of an inorganic surface still requires attention, as different models to explain the charge density distribution can be invoked. More specifically, the fundamental mechanisms that determine the energy levels and work function of these three-component hybrid systems, and how electronic equilibrium is established, need clarification to reliably control interfacial electronic properties in modern opto-electronic devices.

Proposed models to describe the complex inorganic−organic and organic−organic interface processes involve integer charge transfer (ICT),[6,13] induced density of interface states (IDIS),[14] polarization,[15,16] or the formation of charge transfer complexes (CTCs).[10,17,18] In the first experimental work reporting the sequential formation of a π-conjugated organophosphonate monolayer on an inorganic conductor, followed by deposition of a strong electron acceptor, Hanson et al.[19] presumably p-doped the monolayer of quarterthiophene phosphonic acid (4TPA) covalently bound to an indium-tin oxide (ITO) anode surface. They found very high current densities in light emitting devices using the modified ITO anode and assumed that the F_4TCNQ, as the p-type dopant, forms a CTC with the 4TPA molecules, leading to improved charge injection across that interface. In a later theoretical work, Li et al.[17] investigated the impact of F_4TCNQ on an ITO surface modified by a monolayer of *t*-butyl-carbazole-substituted phosphonic acid (t-BCPA, molecular structure shown in Figure 1b) in the framework of density functional theory (DFT) calculations. They assumed that the F_4TCNQ could either form a CTC with the carbazole fragments of the t-BCPA monolayer, or adsorb directly onto the ITO surface while forming a side-

by-side configuration with the t-BCPA molecules; in both cases a substantial increase of the work function was found.

However, taking into account the complexity of the adsorption of a t-BCPA monolayer on the ITO surface and the subsequent deposition of F_4TCNQ, the CTC formation, one of the two configurations assumed in the previous earlier theoretical work,[17] might only represent an extreme case for the adsorption of F_4TCNQ. Due to the wet-chemistry-based modification of inorganic surfaces using a phosphonic acid monolayer,[20,21] there might exist a variety of configurations that make CTC formation competitive or even unfavorable with respect to other mechanisms. For instance, substrate-to-overlayer charge transfer might occur through the molecular interlayer,[22,23] or direct adsorption of F_4TCNQ on the ITO surface (as discussed in Ref.[17]) could happen (with charge transfer between these components) due to interdiffusion through the molecular interlayer.[11]

In the present work, we carried out a joint experimental and theoretical study to further clarify our understanding on the doping and charge transfer mechanisms of such three-component systems, here involving the ITO substrate, the t-BCPA monolayer, and the F_4TCNQ acceptor. Experimentally, X-ray and ultraviolet photoelectron spectroscopy (XPS and UPS), optical absorption (UV/Vis) spectroscopy, and scanning force microscopy (SFM) were applied to study the electronic, optical, and morphological properties of the hybrid systems; theoretically, DFT calculations considering different t-BCPA/F_4TCNQ configurations were performed to provide further insight into the electronic structure, the energy level alignment, and the charge transfer mechanism. In contrast to previous suggestions, we find that p-doping and CTC formation do not occur in these configurations, but that electrons are transferred from ITO to F_4TCNQ, with the t-BCPA monolayer as dielectric in between.

METHODS

Material synthesis. Ultra-smooth ITO films on glass substrates were purchased from Thin Film Devices Inc. (Anaheim, California). First, they were cleaned by a detergent/solvent cleaning procedure, which consisted of scrubbing with a 2% Tergitol® aqueous solution for 5 min, followed by rinsing with deionized water, sonication in 2% Tergitol® aqueous solution for 10 min, copious rinsing and sonication in deionized water for 10 min, and finally sonication in tetrahydrofuran (THF, ≥ 99.9%) for 30 min. After drying in a flow of N_2, the detergent/solvent-cleaned ITO substrates were stored in anhydrous THF until any following investigation and/or preparation. Before surface modification, they were blown dry with N_2 and exposed to UV/ozone under ambient atmosphere for 30 min. The synthesis of the t-butyl-carbazole-substituted PA molecule used for surface modification, namely (3-(3,6-di-tert-butyl-9H-carbazol-9-yl)propyl) phosphonic acid (t-BCPA, see chemical structure in Figure 1b) has been previously published.[24]

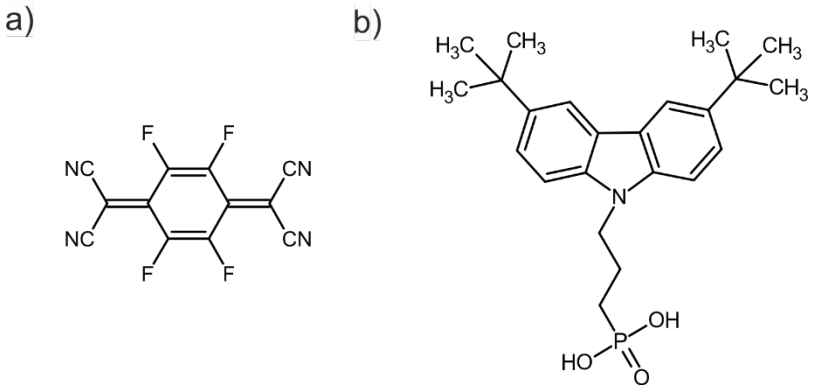

Figure 1. Molecule structure of (a) electron acceptor tetrafluoro-tetracyanoquinodimethane (F_4TCNQ), and (b) electron donor *t*-butyl-carbazole-substituted phosphonic acid (t-BCPA) used for modification of the ITO surface.

Multilayers of t-BCPA molecules were spin-coated from a 1 mg/ml THF (anhydrous) solution at 25 rps, whereas adsorption of t-BCPA molecules to form a phosphonic acid monolayer was carried out by immersion of the ITO substrates in a 1 mM THF (anhydrous) solution for 12 h. The adsorption step was done in a teflon (PTFE) vessel in order to prevent non-specific PA adsorption on the preparation equipment. After immersion, the samples were blown dry with N_2 and annealed on a hot plate under ambient atmosphere at a temperature of 140 °C for 2 h, followed by rinsing in THF for 1 min.

For subsequent molecular acceptor deposition, F_4TCNQ (Sigma-Aldrich, see chemical structure in Figure 1a) was deposited under ultrahigh vacuum (UHV) conditions from a resistively heated quartz crucible. The amount of evaporated molecules was monitored with a quartz crystal microbalance and was set to an evaporation rate equivalent of about 10 Å film mass-thickness per minute, using a density of 1.6 g/cm^3 and assuming the same sticking coefficient on the Au-coated quartz and the (unmodified and t-BCPA-modified) ITO surfaces. A nominal thickness of 40 Å was chosen to represent a closed F_4TCNQ overlayer, due to pronounced island growth of this material on most surfaces.

Scanning force microscopy. Scanning force microscopy (SFM) measurements in intermittent contact mode were performed under ambient conditions using a *NanoWizard 3* (JPK Instruments AG, Germany) instrument. Height and phase images were recorded using aluminium-coated silicon cantilevers (Olympus Corporation, Japan) with a typical resonant frequency of 75 kHz and a spring constant of about 2 N/m. To compensate for thermal drifts and sample inclination, first-order line subtraction and plane correction were applied to the images.

X-ray photoelectron spectroscopy. To prove the stability of the t-BCPA molecules as well as the quality of the corresponding monolayer on ITO, high kinetic energy X-ray photoelectron spectroscopy (HIKE) experiments on the t-BCPA-modified ITO were performed at the high resolution high flux beamline KMC-1 at BESSY synchrotron facility in Berlin (Germany)[25]. The KMC-1 bending magnet beamline uses a high resolution double crystal monochromator with Si(111) crystals. The photoelectron energies were determined using a *Scienta R4000* hemispherical electron kinetic energy analyzer, specifically modified for high transmission and high resolution at kinetic energies up to 10 keV. In our experiments, the monochromator was operated with first order Bragg angles, and an excitation energy of 2.4 keV was used for collecting the molecule-specific core levels C 1s, P 1s (binding energy ~ 2150 eV), and N 1s. The binding energy scale of the core levels were aligned to the position of the Au 4f7/2 core level (84.00 eV) of a reference Au foil. The high-resolution XPS analysis of the C 1s, P 1s and N 1s core level spectra is shown in Figure S1, Supporting Information.

The binding modes of the t-BCPA molecules on the ITO surface were evaluated by analysing the O 1s core level spectrum and its chemical components at the surface. Instead of using the high-energy photon source at the synchrotron, the O 1s core level spectra of both unmodified and t-BCPA-modified ITO were collected with a standard XPS laboratory source (*i.e.*, Al-Kα-radiation, 1486.7 eV) to better resolve the molecule-specific components from those of the ITO substrate. All O 1s core level spectra were recorded at room temperature and normal emission using a hemispherical *Specs Phoibos 100* energy analyzer.

Ultraviolet photoelectron spectroscopy. Ultraviolet photoelectron spectroscopy (UPS) was performed using a helium-gas-discharge lamp (21.218 eV) with low photon flux (attenuated by a Si filter) in order to avoid radiation damage of the samples. The secondary electron cutoff (SECO)

spectra were measured with a sample bias of -10 V. All UPS spectra were recorded at room temperature and normal emission using a hemispherical *Specs Phoibos 100* energy analyzer with 120 meV energy resolution for UPS. Deposited layers of F_4TCNQ on unmodified and t-BCPA-modified ITO surfaces were annealed at 120°C in UHV for 10 min and analysed with UPS in order to investigate the stability of the work function modification, *i.e.*, to check whether the F_4TCNQ molecules are strongly bound to the unmodified and t-BCPA-modified ITO, respectively.

Density functional theory (DFT) calculations. DFT calculations with periodic-boundary conditions were carried out, using the Vienna Ab-Initio Simulation Package (VASP), on unmodified ITO, t-BCPA-modified ITO, and F_4TCNQ/t-BCPA-modified ITO systems, with the projector-augmented wave (PAW) method. The generalized-gradient approximation (GGA) exchange-correlation functional of Perdew, Burke, and Ernzerhof (PBE) was used for geometry optimizations and self-consistent total-energy calculations; in the case of a few representative systems, we also carried out total-energy calculations with the range-separated HSE06 hybrid functional. A repeated-slab approach was adopted with each slab separated by a vacuum space larger than 20 Å and a dipole-correction scheme to cancel any spurious dipole-dipole interactions between non-symmetric slabs along the surface normal direction. The energy cutoff for the plane-waves was set to 300 eV as soft potentials are applied for nitrogen, fluorine, oxygen and carbon atoms. For the geometry optimizations, a Γ-point-only k-mesh was adopted with the Methfessel-Paxton smearing scheme, whereas for total-energy calculations, a Γ-centered 2×2×1 k-mesh was used for Brillouin-zone integrations using the tetrahedron method with Blöchl corrections and a small smearing parameter of 0.05 eV.

The ITO surface was nearly fully passivated by 22 hydrogen atoms per surface unit cell (full passivation would require 24 hydrogens) in order to terminate the dangling bonds of surface

oxygen atoms. The work function of such a model ITO surface is calculated to be 3.53 eV, which is ca. 0.35 eV higher than that of a fully passivated one. We note that a partially hydroxylated ITO surface tends to have a higher work function than a fully hydroxylated one; for instance, a surface with only four surface hydroxyls per surface unit cell has a work function of 4.24 eV;[26] this value is very close to the results measured for the detergent/solvent cleaned (unmodified) ITO substrates (Φ = 4.0 – 4.4 eV) reported in our present UPS experiments (see Figure 6a). However, since experimentally the ITO surfaces are then modified by a t-BCPA monolayer deposited from solution, a t-BCPA-modified ITO model with a higher density of surface hydroxyls appears to be more appropriate in the present case. Thus, we will focus on comparing the impact of F_4TCNQ on the t-BCPA-modified ITO instead of considering the absolute values of work function for unmodified and t-BCPA-modified ITO.

A densely-packed layer of t-BCPA was adsorbed on the ITO surface by assuming a coverage density of 3 PA molecules per surface unit cell (in contrast to the 2 PA molecules per unit cell considered in our earlier work)[17], which is equivalent to 8.45×10^{13} PA molecules/cm^2. The three adsorption sites of t-BCPA on the ITO were selected to render a more homogeneous distribution of the PA molecules on the ITO surface; they correspond to sites 2, 3, and 4 in our earlier work on the adsorption of trifluorophenyl PA molecules on the ITO surface.[27] The geometry of the t-BCPA molecules adsorbed on the ITO was optimized by relaxing both the molecules and the top In-Sn-O layer of the ITO surface. F_4TCNQ molecules were then added on top of the t-BCPA-modified ITO, assuming both low and high coverage (LC/HC) densities (LC = 2.82 and HC = 8.45×10^{13} molecules/cm^2, equivalent to 1 and 3 F_4TCNQ molecules per unit cell) and different adsorption locations. For all geometry optimizations, Van der Waals (vdW) interactions were taken into account based on the DFT-D2 method of Grimme.[28]

RESULTS AND DISCUSSION

1. Surface modification of ITO with t-BCPA

1.1 Surface morphology

The surface morphology of pristine and t-BCPA-modified ITO substrates was imaged by SFM in intermittent contact mode under ambient conditions. The SFM height image of pristine ITO in Figure 2a reveals the presence of small grains with a size of ~ 0.2 µm. Despite the polycrystalline structure, the ITO substrates exhibit a remarkably smooth surface with a roughness (root mean square, rms) of 5.9 Å.

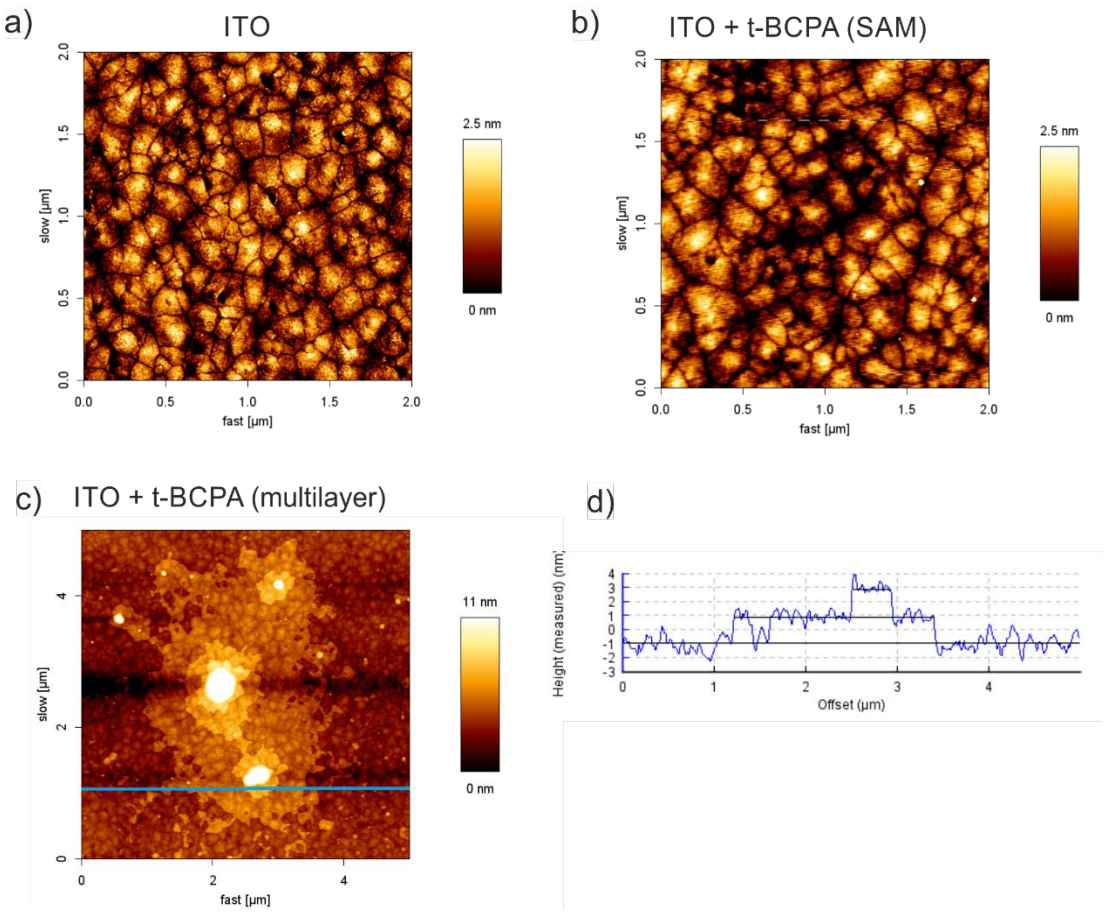

Figure 2. (a) SFM height images of (a) the unmodified ITO surface, the ITO surface modified by (b) t-BCPA-SAM, and (c) spin-coated t-BCPA multilayer; (d) Cross-section along the dotted line in (c).

After surface t-BCPA SAM formation, the morphology of ITO is preserved as visible from the SFM height image in Figure 2b. Overall, the grains of ITO are not masked by the phosphonate layer, and no island and multilayer formation of t-BCPA molecules is apparent. The surface roughness of the t-BCPA-modified ITO surface does not change (rms = 5.8 Å), which is consistent with homogeneous monolayer coverage of t-BCPA on ITO without multilayer formation. For comparison, Figure 2c shows the SFM height image of a spin-coated t-BCPA multilayer on the ITO surface, where much brighter spots corresponding to larger height differences can be observed. The corresponding cross-section analysis in Figure 2d yields steps of multiple t-BCPA layers with a height of ~ 2 nm, thus confirming that the ITO surface modified by a defined t-BCPA SAM (Figure 2b) is uniformly covered with a monolayer of the PA.

1.2 Phosphonic acid binding to ITO

The nature of the PA binding to ITO, along with interactions between neighboring molecules, influences the orientation of the PA organic moiety. In a first step, the adsorption of t-BCPA on ITO was examined at the DFT level. In our earlier work,[17] we considered the binding modes of the PA molecules by removing the two hydrogen atoms of the PO_3H_2 moiety (to form a PO_3 species) before adsorption, which leads to a tridentate binding geometry in the case of two t-BCPA molecules on ITO, with the carbazole molecular planes *parallel* to the surface. Such a configuration then favors the formation of a CTC with a F_4TCNQ molecule coming on top of the carbazole fragment. In the present work, we considered the possibility of a more inclined

orientation of the carbazole fragment of t-BCPA (which is justified by our experimental observations, *vide infra*), as illustrated in the schematic view of the optimized P1−P3 t-BCPA geometries on ITO in Figure 3a (where the subsequently adsorbed F_4TCNQ molecules F1−F3 are also shown).

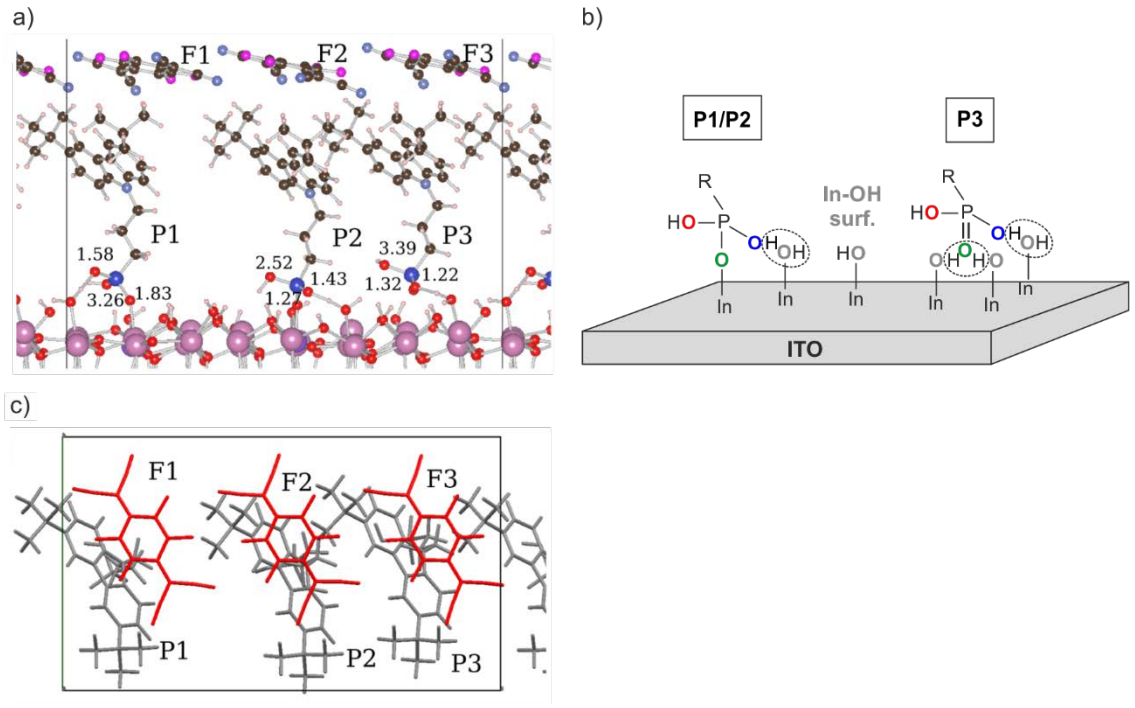

Figure 3. (a) Side and (c) top views of F_4TCNQ deposited on top of the t-BCPA modified ITO surface; the figure illustrates one supercell with high coverage (HC), which includes 3 F_4TCNQ molecules F1–F3 displaying the configuration in-between the t-BCPA molecules; low coverage (LC) corresponds to the presence of only the F2 molecule. Only one In–Sn–O layer of ITO is shown in (a). The purple, grey, brown, blue, red, big pink, and small pink spheres represent F, N, C, P, O, In, and H atoms, respectively. The values shown in black give the DFT-calculated O 1s core-level binding energy shifts (in eV) of the oxygen atoms in the PO_3 moieties with respect to an oxygen in bulk ITO. (b) Schematic illustration of surface−OH groups and calculated PA binding modes on the ITO surface. In (c), the ITO surface is removed to provide a clear view of the

molecular configurations, with the F_4TCNQ and t-BCPA molecules shown in a wire-frame scheme.

The strongly inclined orientation of the carbazole moiety is associated with a monodentate binding mode of the PA on ITO *via* the PO_3H_2 moiety, a scenario that was not considered in our earlier studies.[17] For each of the P1−P3 molecular geometries at the interface, we observe an unreacted P–O–H group (corresponding to the oxygen atoms marked in red in the schematic illustration of the P1/P2 and P3 molecules in Figure 3b). In the case of the P1 and P2 geometries, the binding to ITO occurs *via* an exchange between a single (P–O) bond and a double (P=O) bond, leading to the formation of P–O–In and P–O—H-(OH–In) bondings, with the latter formed via a proton transfer process to a surface hydroxyl (blue oxygen atoms in the P1/P2 geometry in Figure 3b). The oxygen atom of the PA group involved in the P–O–In bond corresponds to the green one in the P1/P2 geometry in Figure 3b, which originally belonged to the P=O group of the molecule. For the P3 geometry, the original P=O group forms two hydrogen bonds with two surface hydroxyls (*i.e.*, P=O—$(OH–In)_2$, corresponding to the green oxygen atom in the P3 geometry in Figure 3b). Simultaneously, a proton transfer occurs between the second P–O–H and a surface hydroxyl group, leading to the formation of a P–O—H-(OH–In) complex (blue oxygen atoms in the P1/P2 and P3 geometries in Figure 3b).

To confirm the monodentate binding mode, we calculated the core-level binding energy shifts (CLBES) for the oxygen atoms belonging to the PO_3H_2 moiety in the t-BCPA monolayer on ITO, with respect to the oxygen atoms in bulk ITO.[27,29] The calculated values of O 1s CLBES (reported in Figure 3a) are all positive which is expected for a monodentate binding mode that makes the PO_3H_2 moiety more stable on the ITO surface.. The CLBES values can be classified

into three groups, a first in the range 1.2 − 1.8 eV (mainly 1.2 − 1.4 eV), a second around 2.5 eV, and a third at ca. 3.3 − 3.4 eV. The lowest CLBES values are associated with the oxygens in P–O–In bonds or P–O–H—(OH–In) complexes, which agrees with the results reported for the P–O–In or hydrogen bonding (P–O—H–O) species in our earlier work.[27] The highest CLBES values of 3.3 − 3.4 eV correspond to the oxygens of the P–O–H groups in the P1 and P3 geometries, which have negligible interactions with the ITO surface. On the other hand, the shift of 2.5 eV appears in the P2 geometry and is due to a weak interaction between the unreacted P–O–H group and the surface hydroxyls (the P–O–H group in the P2 geometry is indeed slightly closer to the surface with respect to the P1 and P3 geometries). Interestingly, the 3.3 – 3.4 eV CLBES associated with the P–O–H groups are very close to the 3.1 eV CLBES value observed experimentally (see discussion below); such a CLBES value was also reported for a fitting component in the experimental O 1s core level of *n*-octylphosphonic acid (OPA) adsorbed on the ITO surface,[30] though the component has not been assigned. The presence of unreacted P–O–H groups upon PA-ITO bonding is also supported by polarization modulation-infrared reflection-adsorption spectroscopy (PM-IRRAS) experiments for *n*-octadecylphosphonic acid (ODPA) bound to ITO.[31]

In a way similar to our previous experimental studies on PA-modified ZnO surfaces,[32,33] the binding modes of t-BCPA molecules to ITO were evaluated via a detailed analysis of the measured O 1s surface components and their energy shifts with respect to the bulk oxygen (*i.e.*, via the CLBES). Figure 4 summarizes the fitting analysis of the O 1s core levels of the pristine (lower panel) and t-BCPA-modified (upper panel) ITO. In the case of the pristine ITO surface, we fitted the experimental O 1s core level spectrum with components previously calculated for ITO by DFT.[30] The three main components of the ITO surface (Figure 4, lower panel) can be attributed to: (i) bulk oxygen (grey component at 530.6 eV, with an asymmetry due to energy-loss

processes),[30] (ii) surface In–O–In (blue component at 531.1 eV), and (iii) surface OH–In (green component at 532.3 eV).

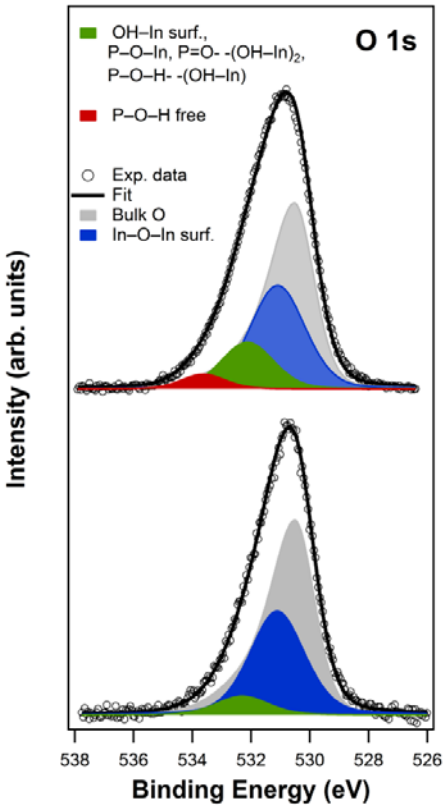

Figure 4. XPS spectra (background subtracted) of the t-BCPA-modified ITO surface: O 1s core level spectra of the pristine (lower panel) and t-BCPA-modified ITO surface (upper panel).

After surface modification (Figure 4, upper panel), the green component is markedly increased, corresponding to an overlap of the signal stemming from surface hydroxyls (OH–In) with new chemical species arising from the monodentate/hydrogen binding of t-BCPA to the ITO surface, related to the formation of the P–O–In bond and P–O–H—(OH–In) / P=O—$(OH–In)_2$ moieties. In addition, a component at higher binding energy (red component at 533.7 eV, *i.e.*, CLBES = 3.1 eV) has to be taken into account to fit the spectrum; such a binding energy shift of

+3.1 eV is consistent with the presence of unreacted P–O–H groups related to the monodentate binding mode, as calculated in the present study (see Figure 3a).

2. Adsorption of F_4TCNQ on t-BCPA-modified ITO

For the adsorption of F_4TCNQ on the t-BCPA-modified ITO surface, i.e., the three-component system, we considered in the calculations either one or three F_4TCNQ molecules per ITO surface unit cell, corresponding to low and high acceptor coverage, respectively. At low coverage, we tested six possible locations of F_4TCNQ, with the acceptor either on top of a t-BCPA molecule or in between two t-BCPA molecules. The calculations show that the total energy difference among the six optimized configurations is less than 0.1 eV per repeat unit with structures where F_4TCNQ is located in-between two t-BCPA molecules (corresponding to the F2 molecule in Figure 3a and c) having a slightly lower total energy than the ones with F_4TCNQ on top of t-BCPA. At high coverage, due to the limited space, we only considered two configurations with the three F_4TCNQ molecules either on top of each t-BCPA molecule or in-between two t-BCPA molecules. As in the case of low coverage, the configuration with F_4TCNQ in-between t-BCPA molecules has a total energy of 0.16 eV lower than the one with F_4TCNQ on top.

Figures 3a and c illustrate the lowest-energy optimized structure of F_4TCNQ on t-BCPA-modified ITO at high coverage, which corresponds to the configuration of three F_4TCNQ molecules in-between the t-BCPA molecules; in this structure, the cyano groups of the F_4TCNQ molecules actually twist out of the ring plane, which was also observed in an earlier work.[17] The lowest-energy geometry for the LC configuration is very similar to the HC configuration, except for the removal of molecules F1 and F3. The adsorption energy (including vdW interactions) per F_4TCNQ molecule on the PA-modified ITO is calculated to be -1.29 eV for LC and -0.88 eV

(average value) for HC; the latter value is smaller due to Coulomb repulsion among negatively charged F_4TCNQ molecules (see more details in the following discussion).

2.2 Charge density redistribution

Changes in the surface electronic properties of the F_4TCNQ/t-BCPA-modified ITO system were investigated by both DFT calculations and UPS measurements. The DFT-calculated work function values of the t-BCPA-modified and F_4TCNQ/t-BCPA-modified ITO (for both HC and LC cases) were determined at both PBE and HSE06 levels. Since the PBE and HSE06 results differ by less than 0.1 eV, here we only discuss the HSE results and compare them with the experimental data. The total work function change $\Delta\Phi$ induced by adsorption of F_4TCNQ molecules onto the t-BCPA-modified ITO is calculated to be very high, i.e., +2.30 eV for HC (Φ = 5.77 eV) and +2.02 eV for LC (Φ = 5.49 eV), respectively (see Figure 5). This high Φ increase is expected to be related to a significant charge density rearrangement in the three-component system, which we now analyze in detail and compare to experiment. We note that the calculated Φ for the F_4TCNQ/t-BCPA-modified ITO at both HC and LC is in good agreement with the experimental value of ~5.6 eV (see Figure 6a).

To understand the correlation between charge transfer and electrostatic potential change (which determines the extent of work function modification), we have evaluated the charge redistribution upon F_4TCNQ adsorption and the electrostatic potential energy of an electron on the F_4TCNQ/t-BCPA-modified ITO surface (see Figures 5a and 5b). Figure 5a shows a contour of the electrostatic potential energy of an electron in the system viewed along the slab *x*-axis for the HC case (within an energy range from -1 to +5 eV); the lower panel of Figure 5b shows the average electrostatic

potential energy within the xy-plane for both the HC and LC cases. The corresponding xy-plane-averaged charge-density difference induced by F_4TCNQ adsorption is displayed in the upper panel of Figure 5b. The largest changes in the averaged charge density occur at two locations: one near the ITO surface (around z ~11 Å) and the other one on F_4TCNQ molecules (around z ~ 25 Å). Across the region where the t-BCPA monolayer lies, the charge-density difference shows first a positive peak and then a negative one of similar amplitude, indicating there occurs a charge redistribution within the t-BCPA monolayer but no net charge transfer from t-BCPA towards the F_4TCNQ molecules. These results underline that a net charge transfer occurs from the ITO surface to the F_4TCNQ molecules with the t-BCPA monolayer acting as a dielectric spacer. This can be further understood by using the simple model presented in Figure 5c (see the discussion below).

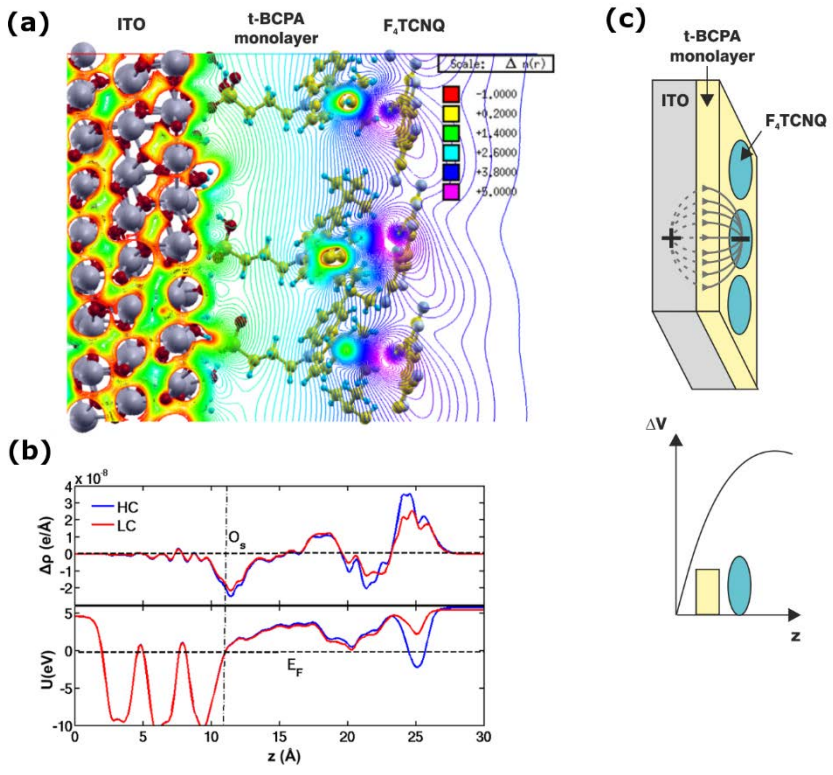

Figure 5. (a) Contour plot of the electrostatic potential energy for the F_4TCNQ/t-BCPA-modified ITO surface; (b) plane-averaged charge density difference (upper panel) and plane-averaged electrostatic potential energy (lower panel); (c) schematic illustration of the electric field lines and the potential drop ΔV as a function of z in the t-BCPA monolayer due to the dipoles formed by charged F4TCNQ molecules in the overlayer (adapted from Ref.[23]).

The amount of charge transfer from the t-BCPA-modified ITO to the F_4TCNQ layer for both the HC and LC cases was obtained by a Bader charge analysis based on charge densities calculated at the HSE06 level for isolated F_4TCNQ molecules, t-BCPA-modified ITO, and F_4TCNQ/t-BCPA-modified ITO surfaces. Table 1 shows the change in the total charge on the F_4TCNQ and t-BCPA molecules upon adsorption of F_4TCNQ on t-BCPA-modified ITO.

Table 1. Change in total charge on the molecules t-BCPA (*i.e.*, geometries P1–P3) and F_4TCNQ (*i.e.*, F1–F3 molecules) induced by adsorption of F_4TCNQ on t-BCPA-modified ITO for the HC and LC cases (see Figure 3); charge transfer Δq from the ITO surface to F_4TCNQ and contribution of the resulting interface dipole $\Delta V_{int.dip}$ to the total work-function change. Negative values represent excess electron charges on the molecules.

Charge (|e|)	t-BCPA			F_4TCNQ			Δq (|e|)	$\Delta V_{int.dip}$ (eV)
	P1 (|e|)	P2(|e|)	P3(|e|)	F1(|e|)	F2(|e|)	F3(|e|)		
HC	+0.06	+0.03	+0.04	-0.18	-0.22	-0.20	-0.47	2.51

LC	+0.04	+0.02	+0.02	--	-0.46	--	-0.38	2.02

The total electron accumulation on the F_4TCNQ molecules in both the HC (-0.60 |e|) and LC (-0.46 |e|) cases is significantly larger than the electron loss on the t-BCPA molecules, which is only +0.13|e| in the HC case and +0.08|e| in the LC case. Thus, the excess negative charge on the F_4TCNQ molecules predominately originate from the ITO surface rather than the t-BCPA SAM. This demonstrates that for the donor (t-BCPA)/acceptor (F_4TCNQ) configurations discussed here there is no significant charge transfer between t-BCPA and F_4TCNQ, a conclusion consistent with the UV/Vis spectroscopy data (see Figures S4 and S5, Supporting Information). Instead, the excess charge on the acceptor molecules are transferred from the ITO substrate through the insulating t-BCPA monolayer. In other words, the ITO surface is p-doped by F_4TCNQ molecules located away from the surface. Similar mechanisms were discussed for a Ag(111) surface pre-covered with physisorbed molecular layers[22,23,34], and subsequent deposition of a thin overlayer of molecular acceptors; [22,23,34] in these studies, electron transfer was found to occur from the metal to the acceptors through the interlayer, with the interlayer remaining neutral.

We note that the negative charge on the more isolated F_4TCNQ in the LC case (-0.46 |e|) is much higher (about twice) than the one on the more densely packed F_4TCNQ in the HC case (ca. -0.2 |e|). This suggests that at a much lower packing density of F_4TCNQ, an “integer” charge transfer (ICT) from the ITO surface to the F_4TCNQ across the insulating t-BCPA monolayer could occur. The amount of charge transfer to F_4TCNQ is in agreement with our experimental findings (*vide infra*).

A simple understanding of the evolution of the energy levels and work function of the system can be obtained by considering the potential drop taking place in between two charged layers. Figure 5c illustrates a previously reported model[23] originally developed for metal-to-overlayer charge transfer. Based on this model, the Φ increase results from an (integer) charge transfer from the substrate to the overlayer through a neutral spacer layer, from ITO to F_4TCNQ in our case, with t-BCPA SAM forming the spacer layer. Since the internal electric field (see Figure 5c) formed with charged F_4TCNQ molecules in the overlayer causes an electrostatic potential decrease (equivalent to an electrostatic potential energy increase for an electron as a test particle) across the spacer layer (*i.e.*, t-BCPA monolayer), the potential energy increase within the t-BCPA monolayer rigidly shifts all the energy levels. The DFT-calculated density of states (DOS) projected to the t-BCPA monolayer (see Figure 7 and its discussion) point towards the role of the electrostatic potential in shifting the energy level of the t-BCPA.

Figure 6 summarizes the UPS data measured for the pristine, t-BCPA-modified, and F_4TCNQ/t-BCPA-modified ITO surfaces. As is common to ITO surfaces that are solvent-cleaned and exposed to air, the work function of pristine ITO was found to vary in a range between 4.0 – 4.4 eV, due to varying surface hydroxyl content and contamination. We thus focus in the following on analyzing the changes in the experimentally obtained work function (ΔΦ) of the systems instead of their absolute values. For each sample investigated, ΔΦ was derived by measuring the work function before and after surface modification.

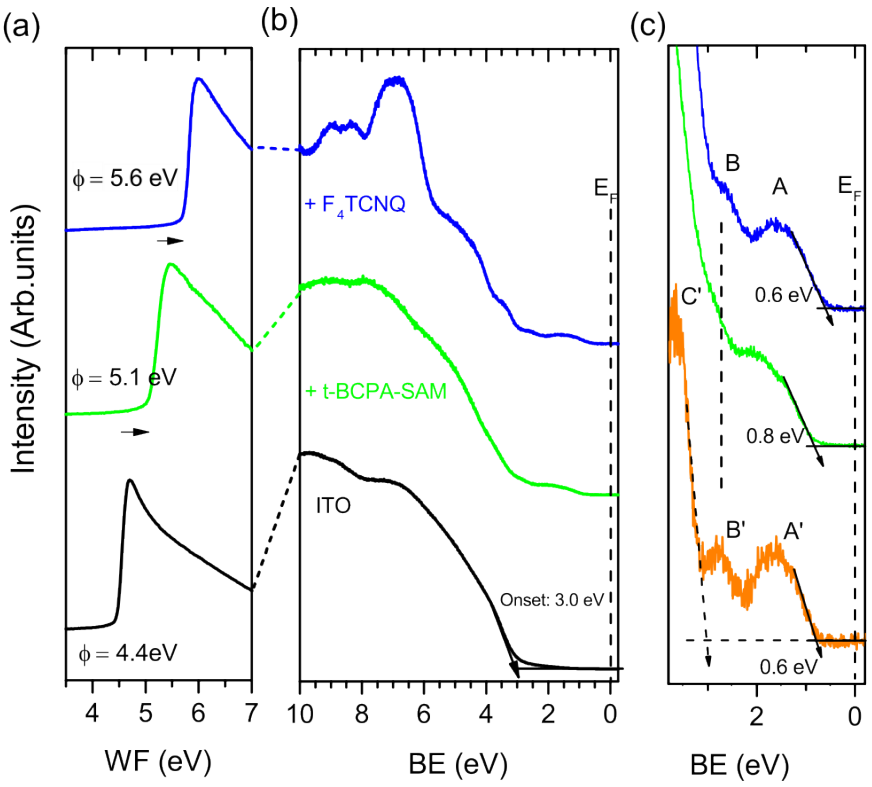

Figure 6. (a) Secondary electron cutoff (SECO) spectra, (b) valence region spectra, and (c) subsequent zooms into the near E_F region, of the pristine and t-BCPA-modified ITO surface, and after deposition of F_4TCNQ, as indicated in the figure. The orange spectrum in (c) corresponds to the difference between the blue and the green spectrum (green spectrum shifted by +0.2 eV), and resembles neutral F_4TCNQ (A') and negatively charged (B' and C') contributions to the valence spectrum.

The formation of the t-BCPA SAM on ITO leads to a $\Delta\Phi \sim +0.7$ eV, as indicated by the secondary electron cutoff (SECO) shift shown in Figure 6a. This measured work function increase differs from the results obtained by DFT calculations (*i.e.*, $\Delta\Phi \sim +0.05$ eV). The main reason is surface composition variation in experiment in contrast to modeling of structurally perfect surfaces with DFT. The experimental situation clearly differs from the ideal case. The situation becomes more reliable when comparing SAM-modified ITO before and after F_4TCNQ deposition, as

samples are kept in vacuum throughout this experimental sequence and the SAM is less affected by ambient exposure than the comparably more reactive pristine ITO surface.

The acceptor F_4TCNQ was then deposited onto the t-BCPA-modified ITO (with a nominal thickness of 40 Å), which induced a substantial Φ increase. As evidenced by the results shown in Figure 5, this Φ increase is associated with electron transfer from the t-BCPA-modified ITO to the F_4TCNQ acceptor molecules. The electron affinity (EA) of F_4TCNQ can be derived from the ionization energy (IE) of 8.3 eV for F_4TCNQ[35] and the optical gap of ~ 3 eV (see Figure S4, Supporting Information), which gives an approximate EA value of 5.3 eV. This value is close to the Φ of the t-BCPA-modified ITO surface. Therefore, electron transfer to the LUMO of F_4TCNQ can be justified based on the simple energy level diagram assuming aligned vacuum energy level for t-BCPA-modified ITO and F_4TCNQ.

Figure 6b and 6c show spectra of the valence region of the pristine, t-BCPA-modified, and F_4TCNQ/t-BCPA-modified ITO surface, respectively. The onsets of the valence band maximum (VBM) of the pristine ITO surface, as well as the position of the highest occupied molecular orbital (HOMO) levels of t-BCPA and F_4TCNQ, respectively, are found by linear extrapolation of the leading edge to zero intensity (see black arrows in Figure 6b and c, respectively). In the present study, the binding energy (BE) of the VBM for pristine (detergent/solvent cleaned) ITO surfaces is in the range 3.0 − 3.2 eV (*e.g.*, black curve in Figure 6b).

The valence region spectrum of the t-BCPA-modified ITO surface (green line in Figure 6b and c) is mainly characterized by an intensity onset at ~ 0.8 eV BE. By comparison with a (spin-coated) t-BCPA multilayer on ITO (not shown), this onset was unambiguously identified as the HOMO level of t-BCPA. After deposition of F_4TCNQ onto the t-BCPA-modified ITO (blue line in Figure

6b), the valence spectrum exhibits additional features. Additional peaks at higher BEs (*i.e.*, ~7 – 10 eV) can be attributed to (neutral) F_4TCNQ molecules.[6] Due to the low sticking coefficient and the high volatility of F_4TCNQ, as well as its tendency to island growth, we assume that the nominal thickness of 40 Å (deposited at room temperature in the present study) does not correspond to a homogeneous F_4TCNQ multilayer (as expected for a layer-by-layer growth), but rather to a (sub-) monolayer coverage,[6] with additional multilayer islands of F_4TCNQ on the t-BCPA SAM. For more insight into the structure of the frontier orbital levels, Figure 6c displays a zoom of the valence region close to the Fermi level E_F. New features are visible (labeled as A and B in Figure 6c) despite the fact that the HOMO of the t-BCPA monolayer overlaps with the new states stemming from the F_4TCNQ overlayer. The emission onset is found at BE ~ 0.6 eV.

The contribution of the F_4TCNQ frontier orbital levels to the valence spectrum can be obtained by subtracting the spectrum of the t-BCPA-modified ITO from that of the F_4TCNQ/t-BCPA-modified ITO surface. Before subtracting the spectra, we shifted the spectrum of t-BCPA-modified ITO by 0.2 eV to lower BE, to account for the electrostatic potential drop across the t-BCPA monolayer as a result of charge transfer between ITO and the acceptors [22,23,34] (see Figure 5c). Furthermore, we re-scaled the spectrum of the t-BCPA-modified ITO by -20 % in intensity, to account for the attenuation due to the F_4TCNQ overlayer. The resulting differential spectrum (orange line in Figure 6c) is characterized by three features, which are labeled as A', B' and C' in Figure 6c. These features in the differential spectrum can be identified by comparison with previously reported UPS spectra of F_4TCNQ deposited on Al_xO_y substrates in the sub-monolayer and multilayer regime (layer formation in low-temperature experiment at -100°C)[6]. While the A' feature corresponds to neutral F_4TCNQ molecules (belonging to multilayer islands), features B' and C' are assigned to negatively charged F_4TCNQ molecules[1,6] at the very interface between the t-BCPA-modified ITO

and F_4TCNQ. These results give direct evidence of negative charge transfer to the acceptor molecules, with the counter-charge residing in ITO (as shown by the DFT results discussed above).

To check the influence of the t-BCPA monolayer on any possible interdiffusion and direct bonding of F_4TCNQ on ITO, the acceptor was also deposited on pristine ITO and t-BCPA-modified ITO, and subsequently annealed at 120°C (see the corresponding SECO and valence spectra in Figures S2 and S3, Supporting Information). As expected for a F_4TCNQ layer on pristine ITO, Φ increased significantly ($\Delta\Phi$ = +1.5 eV, see grey line in Figure S2a) due to charge transfer from the oxide substrate to the acceptors.[6,7] After annealing, the work function remains high, so that almost no change in Φ can be observed (red line in Figure S2a). Accordingly, the valence spectrum after annealing (red line in Figure S2b and 2c) still shows the characteristics of F_4TCNQ on ITO. This suggests that the p-type dopant F_4TCNQ is strongly bound to the bare ITO surface. In contrast, after annealing of the F_4TCNQ/t-BCPA-modified ITO surface the work function decreased again (red line in Figure S3a) and almost recovered the initial value of the t-BCPA-modified ITO. Here, the valence spectrum after annealing (red line in Figure S3b and c) resembles that of the t-BCPA-modified ITO surface again (compare with the green line in Figure 6b) with the HOMO onset of t-BCPA at 0.8 eV. Therefore, we conclude that F_4TCNQ does not strongly bind to the t-BCPA-modified ITO, but remains as a physisorbed overlayer, which can be removed/evaporated at elevated temperatures. Furthermore, this experiment gives us additional evidence that the t-BCPA monolayer is densely packed so that F_4TCNQ molecules cannot diffuse to the ITO surface, where they would bind strongly and keep a high work function even after annealing. Hence, interdiffusion of the two sequentially deposited organic materials t-BCPA and F_4TCNQ can be ruled out.

2.2 Electronic structure details

The electronic structures of the representative HC and LC configurations of F_4TCNQ/t-BCPA-modified ITO and of t-BCPA-modified ITO were calculated at both PBE and HSE06 levels with the HSE results shown in Figure 7. Upon adsorption of F_4TCNQ, the most significant change regarding the valence region is the split and upward energy level shift of the nearly degenerate HOMOs of the t-BCPA molecules, which is induced by charge transfer from ITO to the F_4TCNQ molecules (comparing Figure 7c with a and b). This is also confirmed by the calculated charge density corresponding to the first peak in the projected density of states for t-BCPA in both HC and LC (see Figure 7a, b, and Figure 8a, b). The other important feature in the valence region is the alignment of the LUMO level of F_4TCNQ with the Fermi level of the t-BCPA-modified ITO (see Figure 7a and b). This is also confirmed by the calculated charge density corresponding to the partially occupied PDOS peak crossing the Fermi level, projected to the F_4TCNQ layer (see Figure 8c for the HC case). Pinning of the LUMO of F_4TCNQ, now partially filled with electrons stemming from ITO, is fully consistent with the observation of very similar work functions in the HC and LC cases of F_4TCNQ on t-BCPA-modified ITO surface, and the overall charge transfer.

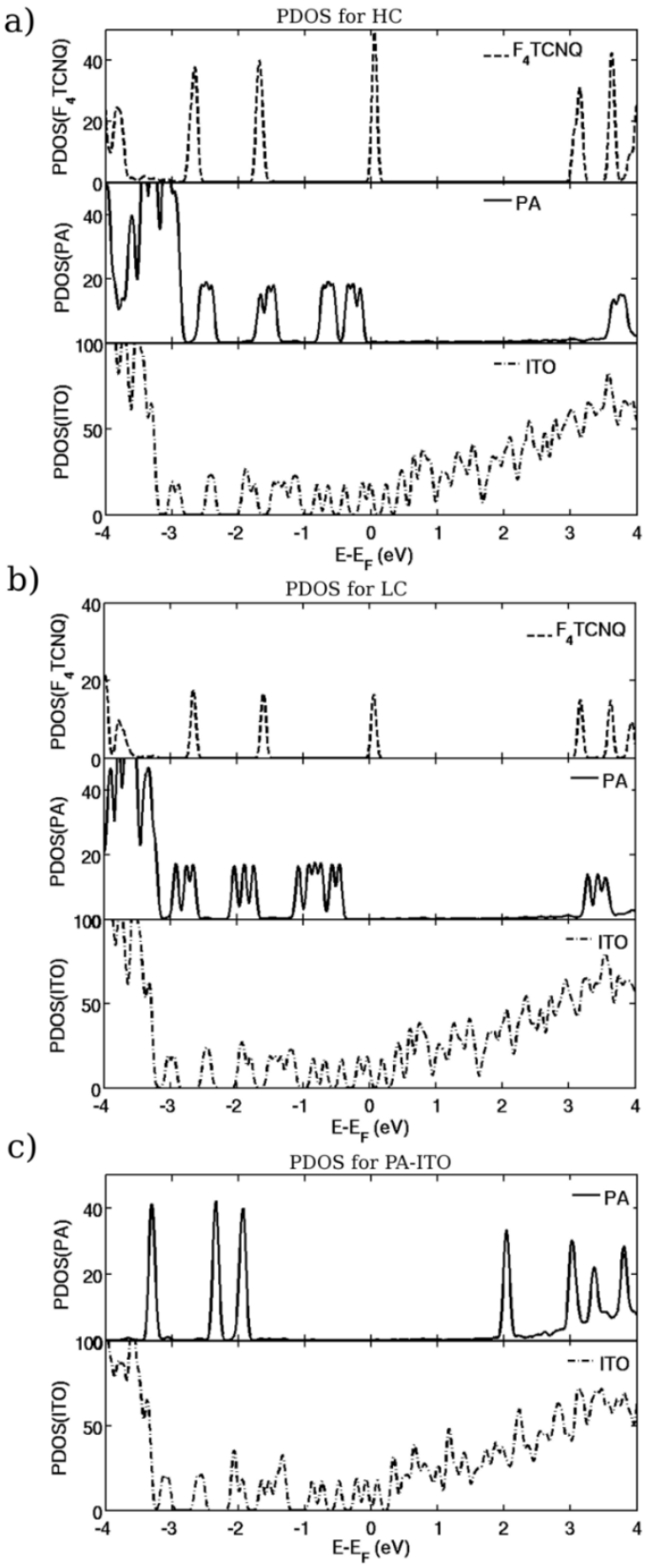
a)
PDOS for HC
PDOS(F4TCNQ)
F4TCNQ
PDOS(PA)
PA
PDOS(ITO)
ITO
E-EF (eV)
b)
PDOS for LC
PDOS(F4TCNQ)
F4TCNQ
PDOS(PA)
PA
PDOS(ITO)
ITO
E-EF (eV)
c)
PDOS for PA-ITO
PDOS(PA)
PA
PDOS(ITO)
ITO
E-EF (eV)

Figure 7. Projected density of states (PDOS) calculated for each component at the HSE06 level in the case of F_4TCNQ/t-BCPA-modified ITO at (a) HC and (b) LC; (c) PDOS for t-BCPA-modified ITO only.

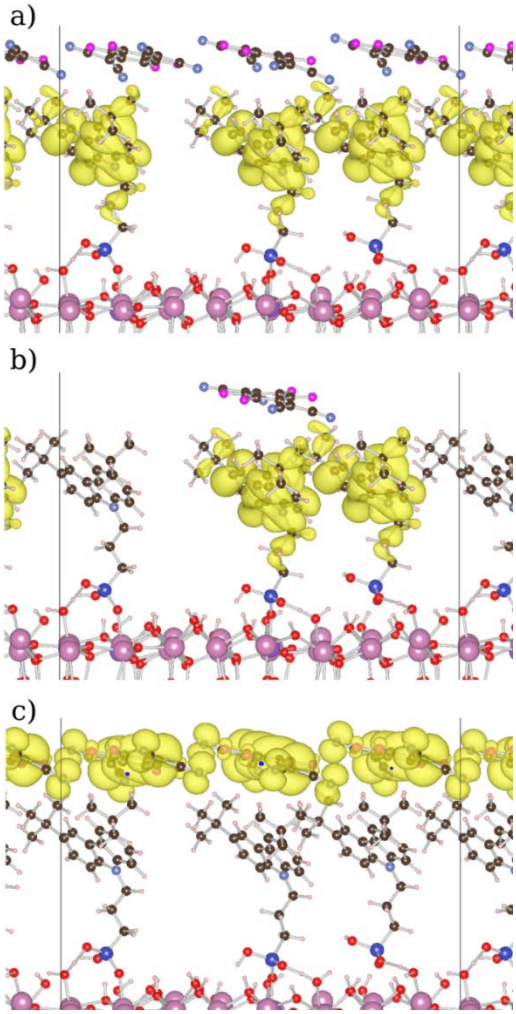

Figure 8. Charge density corresponding to the first occupied PDOS peak within an energy range of ~0.1 eV projected to t-BCPA for the (a) HC and (b) LC cases, and (c) partially occupied PDOS peak crossing the Fermi level projected to F_4TCNQ in the HC case.

CONCLUSIONS

Our combined experimental and theoretical study of a three-component system that is important for advanced electrode engineering in opto-electronic devices reveals a complex charge density redistribution that differs from classical p-type doping but yet significantly impacts the work function. Experimentally, the phosphonic acid- and carbazole-bearing molecule t-BCPA forms a robust and densely packed monolayer on ITO. The experimental and theoretical findings of the PA binding to ITO point towards primarily monodentate binding (*i.e.*, P–O–In) together with hydrogen bonded P–O–H—(OH–In) / P=O—$(OH–In)_2$ complexes formed with one or two surface hydroxyls through a proton transfer process from P–O–H/P=O groups to the surface OH–In. The electron acceptor molecule, F_4TCNQ, significantly increases the work function when deposited on top of the t-BCPA-modified ITO. This originates from electron transfer to the acceptor, evidenced by the spectral signature of negatively charged F_4TCNQ molecules in UPS. This is fully consistent with the results of the DFT calculations, which reveal that the excess electron charge on the acceptors comes from the ITO substrate and that p-doping of the π-conjugated carbazole PA moiety does not occur. Thus, the SAM itself remains essentially charge neutral but experiences the electrostatic field generated by the charges appearing on the ITO surface and the F_4TCNQ layer.

A previous experimental study[19] using a similar (π-conjugated) phosphonate monolayer and subsequent deposition of the acceptor F_4TCNQ has demonstrated the efficacy of this approach to modify the surface of ITO anodes, and to improve device performances due to improved charge

injection and increased current densities. Our present findings on the origin of work function increase and the energy level alignment of such multi-component systems for advanced surface modification will aid in future design of surface modifiers for organic electronics applications, enabling reaching a higher range of accessible work function values and thus better ohmic contacts.

ASSOCIATED CONTENT

Supporting Information. XPS C 1s, P 1s and N 1s core level spectra (Figure S1), UPS spectra of annealed samples (Figure S2 and S3), UV/Vis absorption spectra of (pure and mixed) organic molecules (Figure S4 and S5).

AUTHOR INFORMATION

Corresponding Authors

*E-mail: mtimpel@physik.hu-berlin.de

*E-mail: hong.li@chemistry.gatech.edu

Author Contributions

The manuscript was written through contributions of all authors. All authors have given approval to the final version of the manuscript. Δ These authors contributed equally.

Funding Sources

Notes

The authors declare no competing financial interest.

ACKNOWLEDGMENT

The work in Berlin was supported by the SFB951 (DFG), the European Commission FP7 Project HYMEC (Grant No. 263073), and the Helmholtz-Energie-Allianz “Hybrid-Photovoltaik”. The work in Atlanta was supported by the Office of Naval Research under Award No. N00014-17-1-2208 and the Georgia Research Alliance.

REFERENCES

(1) Koch, N.; Duhm, S.; Rabe, J. P.; Vollmer, A.; Johnson, R. L. Optimized Hole Injection with Strong Electron Acceptors at Organic-Metal Interfaces. *Phys. Rev. Lett.* **2005**, *95* (23), 237601.

(2) Romaner, L.; Heimel, G.; Brédas, J.-L.; Gerlach, A.; Schreiber, F.; Johnson, R. L.; Zegenhagen, J.; Duhm, S.; Koch, N.; Zojer, E. Impact of Bidirectional Charge Transfer and Molecular Distortions on the Electronic Structure of a Metal-Organic Interface. *Phys. Rev. Lett.* **2007**, *99* (25), 256801.

(3) Rangger, G. M.; Hofmann, O. T.; Romaner, L.; Heimel, G.; Bröker, B.; Blum, R. P.; Johnson, R. L.; Koch, N.; Zojer, E. F4TCNQ on Cu, Ag, and Au as Prototypical Example for a Strong Organic Acceptor on Coinage Metals. *Phys. Rev. B - Condens. Matter Mater. Phys.* **2009**, *79* (16), 1–12.

(4) Chen, W.; Chen, S.; Qi, D. C.; Gao, X. Y.; Wee, A. T. S. Surface Transfer P-Type Doping of Epitaxial Graphene. *J. Am. Chem. Soc.* **2007**, *129* (34), 10418–10422.

(5) Coletti, C.; Riedl, C.; Lee, D. S.; Krauss, B.; Patthey, L.; von Klitzing, K.; Smet, J. H.; Starke, U. Charge Neutrality and Band-Gap Tuning of Epitaxial Graphene on SiC by Molecular Doping. *Phys. Rev. B* **2010**, *81* (23), 235401.

(6) Braun, S.; Salaneck, W. R. Fermi Level Pinning at Interfaces with Tetrafluorotetracyanoquinodimethane (F4-TCNQ): The Role of Integer Charge Transfer States. *Chem. Phys. Lett.* **2007**, *438* (4–6), 259–262.

(7) Schlesinger, R.; Xu, Y.; Hofmann, O. T.; Winkler, S.; Frisch, J.; Niederhausen, J.; Vollmer, A.; Blumstengel, S.; Henneberger, F.; Rinke, P.; et al. Controlling the Work Function of ZnO and the Energy-Level Alignment at the Interface to Organic Semiconductors with a Molecular Electron Acceptor. *Phys. Rev. B* **2013**, *87* (15), 155311.

(8) Winkler, S.; Frisch, J.; Schlesinger, R.; Oehzelt, M.; Rieger, R.; Räder, J.; Rabe, J. P.; Müllen, K.; Koch, N. The Impact of Local Work Function Variations on Fermi Level Pinning of Organic Semiconductors. *J. Phys. Chem. C* **2013**, *117*, 22285–22289.

(9) Drechsel, J.; Pfeiffer, M.; Zhou, X.; Nollau, A.; Leo, K. Organic Mip-Diodes by P-Doping of Amorphous Wide-Gap Semiconductors: CV and Impedance Spectroscopy. *Synth. Met.* **2002**, *127*, 201–205.

(10) Méndez, H.; Heimel, G.; Opitz, A.; Sauer, K.; Barkowski, P.; Oehzelt, M.; Soeda, J.; Okamoto, T.; Takeya, J.; Arlin, J.-B.; et al. Doping of Organic Semiconductors: Impact of Dopant Strength and Electronic Coupling. *Angew. Chemie* **2013**, *125* (30), 7905–7909.

(11) Duhm, S.; Salzmann, I.; Bröker, B.; Glowatzki, H.; Johnson, R. L.; Koch, N. Interdiffusion of Molecular Acceptors through Organic Layers to Metal Substrates Mimics Doping-Related Energy Level Shifts. *Appl. Phys. Lett.* **2009**, *95* (9), 2009–2011.

(12) Walzer, K.; Männig, B.; Pfeiffer, M.; Leo, K. Highly Efficient Organic Devices Based on Electrically Doped Transport Layers. *Chem. Rev.* **2007**, *107* (4), 1233–1271.

(13) Braun, S.; Salaneck, W. R.; Fahlman, M. Energy-Level Alignment at Organic/Metal and Organic/Organic Interfaces. *Adv. Mater.* **2009**, *21* (14–15), 1450–1472.

(14) Vázquez, H.; Oszwaldowski, R.; Pou, P.; Ortega, J.; Pérez, R.; Flores, F.; Kahn, A. Dipole Formation at metal/PTCDA Interfaces: Role of the Charge Neutrality Level. *Europhys. Lett.* **2004**, *65* (6), 802–808.

(15) Avilov, I.; Geskin, V.; Cornil, J. Quantum-Chemical Characterization of the Origin of Dipole Formation at Molecular Organic/organic Interfaces. *Adv. Funct. Mater.* **2009**, *19* (4), 624–633.

(16) Verlaak, S.; Beljonne, D.; Cheyns, D.; Rolin, C.; Linares, M.; Castet, F.; Cornil, J.; Heremans, P. Electronic Structure and Geminate Pair Energetics at Organic-Organic Interfaces: The Case of Pentacene/ C60 Heterojunctions. *Adv. Funct. Mater.* **2009**, *19* (23), 3809–3814.

(17) Li, H.; Winget, P.; Bredas, J.-L. Surface Modification of Indium-Tin-Oxide via Self-Assembly of a Donor-Acceptor Complex: A Density Functional Theory Study. *Adv. Mater.* **2012**, *24* (5), 687–693.

(18) Méndez, H.; Heimel, G.; Winkler, S.; Frisch, J.; Opitz, A.; Sauer, K.; Wegner, B.; Oehzelt, M.; Röthel, C.; Duhm, S.; et al. Charge-Transfer Crystallites as Molecular Electrical Dopants. *Nat. Commun.* **2015**, *6*, 8560.

(19) Hanson, E. L.; Guo, J.; Koch, N.; Schwartz, J.; Bernasek, S. L. Modification of Indium Tin Oxide for Improved Charge Injection in Organic Devices. *J. Am. Chem. Soc.* **2005**, *127* (28), 10058–10062.

(20) Hotchkiss, P. J.; Jones, S. C.; Paniagua, S. A.; Sharma, A.; Kippelen, B.; Armstrong, N. R.; Marder, S. R. The Modification of Indium Tin Oxide with Phosphonic Acids: Mechanism of Binding, Tuning of Surface Properties, and Potential for Use in Organic Electronic Applications. *Acc. Chem. Res.* **2012**, *45* (3), 337–346.

(21) Paniagua, S. a; Li, E. L.; Marder, S. R. Adsorption Studies of a Phosphonic Acid on ITO: Film Coverage, Purity, and Induced Electronic Structure Changes. *Phys. Chem. Chem. Phys.* **2014**, *16* (7), 2874–2881.

(22) Amsalem, P.; Niederhausen, J. Metal-to-Acceptor Charge Transfer through a Molecular Spacer Layer. *J. Phys. Chem. C* **2011**, *115*, 17503–17507.

(23) Amsalem, P.; Niederhausen, J.; Wilke, A.; Heimel, G.; Schlesinger, R.; Winkler, S.; Vollmer, A.; Rabe, J. P.; Koch, N. Role of Charge Transfer, Dipole-Dipole Interactions,

and Electrostatics in Fermi-Level Pinning at a Molecular Heterojunction on a Metal Surface. *Phys. Rev. B* **2013**, *87* (3), 35440.

(24) Hotchkiss, P. J. Design, Synthesis, and Use of Phosponic Acids for the Surface Modification of Metal Oxides, 2008.

(25) Gorgoi, M.; Svensson, S.; Schäfers, F.; Öhrwall, G.; Mertin, M.; Bressler, P.; Karis, O.; Siegbahn, H.; Sandell, A.; Rensmo, H.; et al. The High Kinetic Energy Photoelectron Spectroscopy Facility at BESSY Progress and First Results. *Nucl. Instruments Methods Phys. Res. A* **2009**, *601* (1–2), 48–53.

(26) Li, H.; Winget, P.; Brédas, J.-L. Transparent Conducting Oxides of Relevance to Organic Electronics: Electronic Structures of Their Interfaces with Organic Layers. *Chem. Mater.* **2014**, *26* (1), 631–646.

(27) Li, H.; Paramonov, P.; Brédas, J.-L. Theoretical Study of the Surface Modification of Indium Tin Oxide with Trifluorophenyl Phosphonic Acid Molecules: Impact of Coverage Density and Binding Geometry. *J. Mater. Chem.* **2010**, *20* (13), 2630–2637.

(28) Grimme, S. Semiempirical GGA-Type Density Functional Constructed with a Long-Range Dispersion Correction. *J. Comput. Chem.* **2006**, *27*, 1787–1799.

(29) Wood, C.; Li, H.; Winget, P.; Brédas, J.-L. Binding Modes of Fluorinated Benzylphosphonic Acids on the Polar ZnO Surface and Impact on Work Function. *J. Phys. Chem. C* **2012**, *116* (36), 19125–19133.

(30) Paramonov, P. B.; Paniagua, S. A.; Hotchkiss, P. J.; Jones, S. C.; Armstrong, N. R.; Marder, S. R.; Brédas, J.-L. Theoretical Characterization of the Indium Tin Oxide Surface and of Its Binding Sites for Adsorption of Phosphonic Acid Monolayers. *Chem. Mater.* **2008**, *20*, 5131–5133.

(31) Paniagua, S. A.; Hotchkiss, P. J.; Jones, S. C.; Marder, S. R.; Mudalige, A.; Marrikar, F. S.; Pemberton, J. E.; Armstrong, N. R. Phosphonic Acid Modification of Indium-Tin Oxide Electrodes : Combined XPS / UPS / Contact Angle Studies. *J Phys Chem C* **2008**, *112*, 7809–7817.

(32) Timpel, M.; Nardi, M. V; Krause, S.; Ligorio, G.; Christodoulou, C.; Pasquali, L.; Giglia, A.; Frisch, J.; Wegner, B.; Moras, P.; et al. Surface Modification of ZnO(0001)−Zn with Phosphonate-Based Self-Assembled Monolayers: Binding Modes, Orientation and Work Function. *Chem. Mater.* **2014**, *26*, 5042−5050.

(33) Timpel, M.; Nardi, M. V.; Ligorio, G.; Wegner, B.; Pätzel, M.; Kobin, B.; Hecht, S.; Koch, N. Energy-Level Engineering at ZnO/Oligophenylene Interfaces with Phosphonate-Based Self-Assembled Monolayers. *ACS Appl. Mater. Interfaces* **2015**, *7* (22), 11900–11907.

(34) Niederhausen, J.; Amsalem, P.; Wilke, A.; Schlesinger, R.; Winkler, S.; Vollmer, A.; Rabe, J. P.; Koch, N. Doping of C 60 (Sub)monolayers by Fermi-Level Pinning Induced Electron Transfer. *Phys. Rev. B - Condens. Matter Mater. Phys.* **2012**, *86* (8), 1–5.

(35) Kahn, A.; Koch, N.; Gao, W. Electronic Structure and Electrical Properties of Interfaces between Metals and Pi-Conjugated Molecular Films. *J. Polym. Sci.* **2003**, *41*, 2529–2548.